Giant temperature-independent ultraviolet circular dichroism in Co_2MnX (X = Ga,Ge) Heusler magnetic thin films

Yao Zhang,[1,2,*] Jie Sung,[3] Yuefeng Yin,[4,5] Yu-Ying Chang,[3] Nikhil V. Medhekar,[4,5] Simon Granville,[1,2,†] and Hua-Shu Hsu[3,‡]

[1] *Robinson Research Institute, Victoria University of Wellington, Wellington 6140, New Zealand*
[2] *MacDiarmid Institute for Advanced Materials and Nanotechnology, Wellington 6011, New Zealand*
[3] *Department of Applied Physics, National Pingtung University, No. 4–18 Minsheng Rd., Pingtung 90003, Taiwan*
[4] *Department of Materials Science and Engineering, Monash University, Clayton, Victoria 3800, Australia*
[5] *ARC Centre of Excellence in Future Low-Energy Electronics Technologies, Clayton, Victoria 3800, Australia*

(Received 31 October 2024; revised 16 July 2025; accepted 28 August 2025; published 19 September 2025)

Optical circular dichroism (CD) is a useful method for investigating the role of chirality in natural and physical processes. A large magnitude of CD must be achieved for spectroscopy and sensing, particularly in the ultraviolet (UV) energy range where molecular chirality is identifiable. However, the strong absorption of UV wavelengths in many materials precludes large UV-CD responses. In this work, we observed a giant temperature-independent magnetic circular dichroism (MCD) in the UV regime in magnetic Co_2MnGa thin films. We demonstrated the MCD in this system is controlled by the magnetization and originates from the hybridization of Co and Mn 3*d* states, by referring to calculations of the spin-polarized density of states. Based on these results, we propose and test two general rules for identifying other magnetic materials expected to have large MCD. Our results open a route towards finding magnetic materials with large MCD excited at different energy ranges, for CD applications with immunity to temperature variation.

DOI: 10.1103/h822-rw47

I. INTRODUCTION

Chirality is a fundamental material property of great significance to understanding and controlling phenomena in physics, chemistry, and the biological sciences [1,2]. Chiral molecules, nanoparticles, and crystals can also be used in unique physical properties and applications [3–5], so having a convenient method of measuring chirality in materials is essential. Circular dichroism (CD), defined as the absorption difference between right-handed circularly polarized (RCP) and left-handed circularly polarized (LCP) light, is widely used in the characterization of chiral molecules [1]. Chiral molecules usually exhibit a chiral optical response in the ultraviolet (UV) regime [6]. This optical response is intrinsically small due to the weak interaction between the magnetic component of light and the chiral molecules [7,8]. Thus, high analyte concentration and long integration time is required for chiral molecule sensing by CD spectroscopy [9,10].

Generating a large UV-CD magnitude in CD spectroscopy is highly desirable to enhance sensing sensitivity and improve detectability for spectroscopy. Currently, large CD in the visible and near-infrared regime has been obtained in metals with metasurfaces (periodic subwavelength structures). Metasurfaces create or enhance the surface plasmon resonances, which interact with chiral molecules and thus detect them [11,12]. However, the UV-CD value in these nanostructures is very weak, below 10 mdeg [6], due to the strong absorption of UV light in the metals [13–15]. Also, advanced nanofabrication techniques are required to make these metasurfaces [16]. Furthermore, the CD caused by such metasurfaces is not easy to further manipulate using an external stimulus, which would be a useful characteristic for CD spectroscopy [17,18].

A CD signal can also be generated in magnetic materials due to the magneto-optical effect resulting from the spin-polarized band structure, in which the spin-polarized electrons can be selectively excited by the polarized light from occupied bands to unoccupied bands, as shown in Fig. 1(a) [19]. The LCP and RCP light can be absorbed in energy transitions between the spin minority ↓ and spin majority ↑ electron states. A difference of the LCP and RCP absorptions arises because the internal exchange field breaks the degeneracy of the minority and majority electronic states, leading to different transition probabilities for the two

*Contact author: yao.zhang@vuw.ac.nz
†Contact author: simon.granville@vuw.ac.nz
‡Contact author: hshsu@mail.nptu.edu.tw

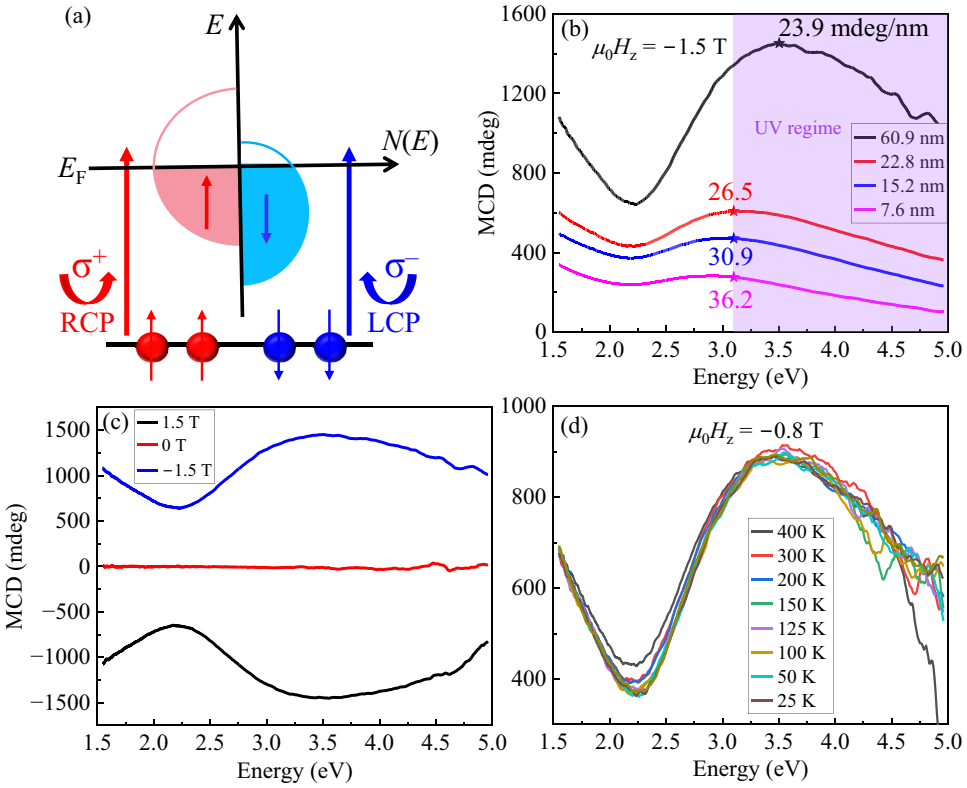

FIG. 1. MCD characterization for Co_2MnGa thin films. (a) Schematic diagram of MCD effect resulting from the spin-polarized electronic band structure. The LCP and RCP light excites transitions between the (occupied and unoccupied) spin minority ↓ and spin majority ↑ states, respectively. (b) MCD at 300 K as a function of excitation energy for 7.6, 15.2, 22.8, and 60.9 nm Co_2MnGa films in a −1.5 T external magnetic field. (c) MCD at 300 K as a function of excitation energy for 60.9 nm Co_2MnGa in −1.5, 0, and 1.5 T. (d) Temperature dependence of MCD for 60.9 nm Co_2MnGa in −0.8 T.

polarizations. Though the overall UV light-intensity loss still happens in magnetic metallic materials, they can still generate a significant CD. By preparing chiral-molecule layers on magnetic thin films, spin-polarized electrons from the magnetic material can diffuse into the chiral-molecule layers. These chiral molecules act as spin filters, selectively transmitting electrons with one spin orientation while reflecting or scattering those with the opposite spin—a phenomenon known as the chiral-induced spin selectivity (CISS) effect—which offers a promising approach for identifying chiral molecules [2]. Furthermore, the spin-polarized electronic states that lead to the CD relate to the magnetization, which can be reversed by the magnetic field so that the CD magnitude and polarization can be easily tuned, which is called magnetic circular dichroism (MCD) [20].

The MCD effect has been investigated in magnetic materials before, such as in ferromagnetic transition metals and their alloys [21,22] and in Fe-containing garnets [23]. However, the MCD signal of these is either very small or displays poor thermal stability in the UV regime. Several works report that combining magnetic materials with metasurfaces [24–27] can be used to enhance and engineer the UV-CD signal. However, the enhancement of CD in those systems is mostly in the visible or near-infrared regime.

In this work, we observed a giant temperature-independent UV MCD reaching 1450 mdeg in a 60.9-nm ferromagnetic Co_2MnGa thin film. The MCD relates to the magnetization so that it can be tuned to the opposite polarization by a magnetic field. We demonstrated that the MCD in Co_2MnGa is determined by the spin-polarized band structure. Finally, we proposed and tested two rules to use when searching for magnetic materials with large MCD.

II. EXPERIMENTAL SECTION

Sample preparation: following our previous work [28–33] Co_2MnGa and Co_2MnGe thin films were epitaxially deposited on double-side-polished MgO(001) substrates in a Kurt J Lesker CMS-18 magnetron sputtering system with a base pressure below 3×10^{-8} Torr. Before fabricating thin films, substrates were cleaned with an Ar plasma, and then annealed at 400 °C for 30 min in the vacuum chamber. Co_2MnGa and Co_2MnGe thin films were each dc magnetron sputtered from a stoichiometric polycrystalline

target at 100 W under 6 mTorr of Ar, with the substrates held at 400 °C while the sample holder was rotated at 20 rpm. The growth rate was calibrated by x-ray reflectivity measurements. A $Co_2MnGa_{0.5}Ge_{0.5}$ film was grown by cosputtering from the Co_2MnGa and Co_2MnGe targets. All samples were postannealed *in situ* at 400 °C for 20 min to improve the lattice structure and the atomic ordering among Co, Mn, and Ga/Ge sites. After cooling down to ambient temperature, a 3-nm protective Ta layer was deposited on the top. The composition has been confirmed by x-ray fluorescence.

MCD measurements: the MCD signals were measured using a Jasco J-815 MCD spectrometer equipped with a 450-W xenon lamp as a white light source. The natural unpolarized light was irradiated into the monochromator using a linear polarizer and converted into a specific energy. After traversing through the photoelastic modulator, the linearly polarized light was decomposed into two circularly polarized rays (σ^+ and σ^-). Both rays were simultaneously shone on the samples, and the spot size was approximately 4 mm^2. The power density of the applied light excitation was 9 $\mu W/cm^2$. After they interact with the sample, the changes in the two circularly polarized rays were detected using a photomultiplier. To control the magnetization of the thin film, a variable magnetic field was applied along the light incident direction [34]. The MCD signal of the MgO substrate is very small and has been subtracted for all MCD results (see the Supplemental Material [35]).

Electrical transport measurements: samples were patterned into standard Hall bars ($l = 500$ μm, $w = 50$ μm) by photolithography and then Ar ion milling for magnetotransport characterization. The transport measurements were performed using the resistivity option of a Physical Property Measurement System (PPMS, Quantum Design).

Band-structure calculation: we used density-functional theory (DFT), within the generalized gradient approximation (GGA), as implemented in the Vienna *ab initio* simulation package (VASP), to calculate the electronic structure of Co_2MnGa and Co_2MnGe [36].

III. RESULTS

A. MCD characterization

MCD measurements were done at 300 K for Co_2MnGa thin films (thicknesses 7.6–60.9 nm) excited with light from 1.55 to 4.96 eV with a magnetic field applied normal to the surface of the films. Figure 1(b) shows the MCD curves for the Co_2MnGa films at a fixed magnetic field of −1.5 T. At this magnetic-field intensity, the Co_2MnGa films have magnetizations nearly saturated along the (out-of-plane) field direction.

Broadband MCD signals can be observed from the near infrared to UV. The shape of the curves for all thicknesses is similar, but the MCD magnitude decreases by reducing the thickness. The CD spectra are defined as

$$\theta = \frac{\ln 10}{4}(A_{RCP} - A_{LCP})\frac{180}{\pi}(\text{degree}) \text{ [34, 36]}, \quad (1)$$

where θ is the ellipticity of the polarization light, A_{RCP} and A_{LCP} are the optical absorption of samples under RCP and LCP light illuminations, respectively. A giant value for MCD, 1450 mdeg, can be observed for 60.9-nm Co_2MnGa at 3.50 eV in the UV range, which is an order of magnitude higher than the MCD in classic magnetic transition metals such as Co [22]. The highest thickness-normalized MCD in the UV range is 36.2 mdeg/nm for the 7.6-nm thin film, around 3.2 eV. Figure 1(c) shows the MCD curves of the 60.9-nm Co_2MnGa thin film in fields of 1.5, 0, and −1.5 T. The MCD signal is reversed by reversing the magnetic field and no signal can be observed in zero magnetic field. All these suggest that MCD is related to the magnetic behavior of the Co_2MnGa. The Curie temperature of Co_2MnGa is around 700 K [38], higher than the maximum 400 K of our MCD measurements, so in our experiments

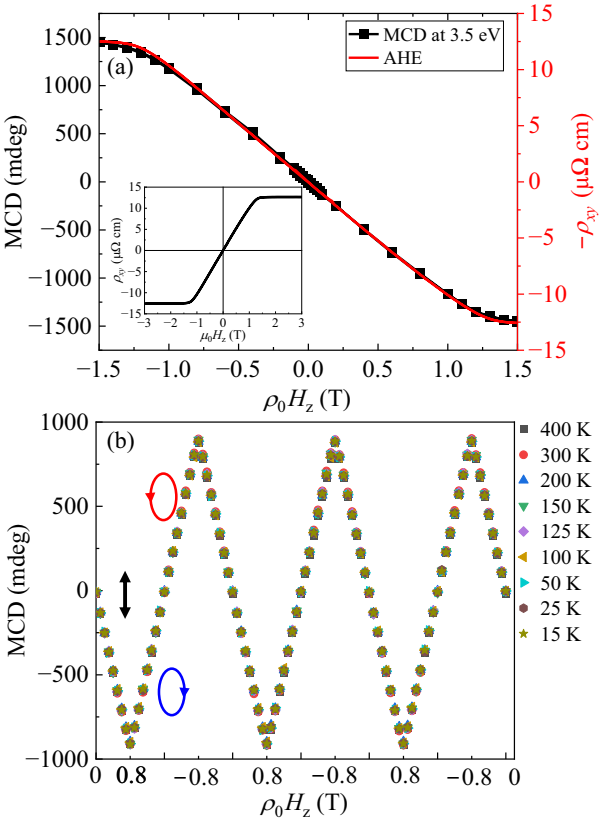

FIG. 2. Magnetic-field dependence of MCD for 60.9 Co_2MnGa thin film. The optical excitation energy is 3.5 eV. (a) MCD and negative of the anomalous Hall effect measured by sweeping the magnetic field from −1.5 to 1.5 T at 300 K. The inset is the raw anomalous Hall effect curve over the full range of fields. (b) Three cycles of magnetic-field dependence of MCD at various temperatures from 15 to 400 K.

the film magnetic moment and static density of electronic states do not change too much. However, the MCD signal, which involves excitations between electronic states, is usually sensitive to the temperature [39]. For our thin films, the MCD is remarkably temperature independent from 400 to 15 K [see Fig. 1(d)] over the full range of photon energies.

B. Relationship of MCD and magnetization

To investigate the relationship of MCD and Co_2MnGa magnetization, we measure the MCD of the 60.9-nm Co_2MnGa film by sweeping the out-of-plane magnetic field from −1.5 to 1.5 T with a fixed 3.50-eV excitation energy, as shown in Fig. 2(a).

An approximately linear dependence of MCD on magnetic field can be observed from −0.8 to 0.8 T. Then, the signal is saturated at 1.5 T. Also plotted in Fig. 2(a) is the anomalous Hall effect (AHE) measured from the film. The MCD has the opposite sign to the AHE, but the shape of the magnetic-field dependence of MCD perfectly matches the AHE curve, which is well known to characterize the field dependence of the magnetization [28,40–43]. Thanks to this relationship, the MCD value can be significantly tuned from 1450 mdeg to −1450 mdeg using the magnetic field. To test the linear field dependence, we did three cycles of magnetic field sweeping between −0.8 and 0.8 T at various temperatures, as shown in Fig. 2(b). One can see a near perfect linear dependence of MCD signal on the magnetic field. The polarization of MCD is linear at zero magnetic field, left-hand elliptical at negative field, and right-hand elliptical at positive field.

C. Spin-polarized density of states calculation

To investigate the electronic states that are the origin of the MCD in our thin films, we calculated the spin-polarized density of states (DOS) of Co_2MnGa. Figure 3 shows the partial DOS of the 3*d* states as the contributions of the 1*s* and 2*p* states in this energy range are negligible. Unlike x-ray MCD (XMCD) in which the signal arises from the excitation of a core electron [44], such as the 2*p* states, our optical MCD excites electrons from the valence bands into unoccupied conduction bands.

One can see that there are two regions of large DOS in the unoccupied minority spin states around 1.0 and 1.7 eV above the Fermi level. These are due to the hybridization of t_{2g} and e_g Co and Mn 3*d* states, as shown in Figs. 3(b) and 3(c). In contrast, there is only a small and featureless DOS in the majority states from Fermi level up to 4 eV. For MCD in the visible-UV range, electronic transitions must be available between filled (below 0 eV) and empty (above 0 eV) states, where the energy difference of the states matches the photon energy. So, in the visible-UV range, spin-polarized optical transitions will be dominated by the minority spin states. Because MCD(total) =

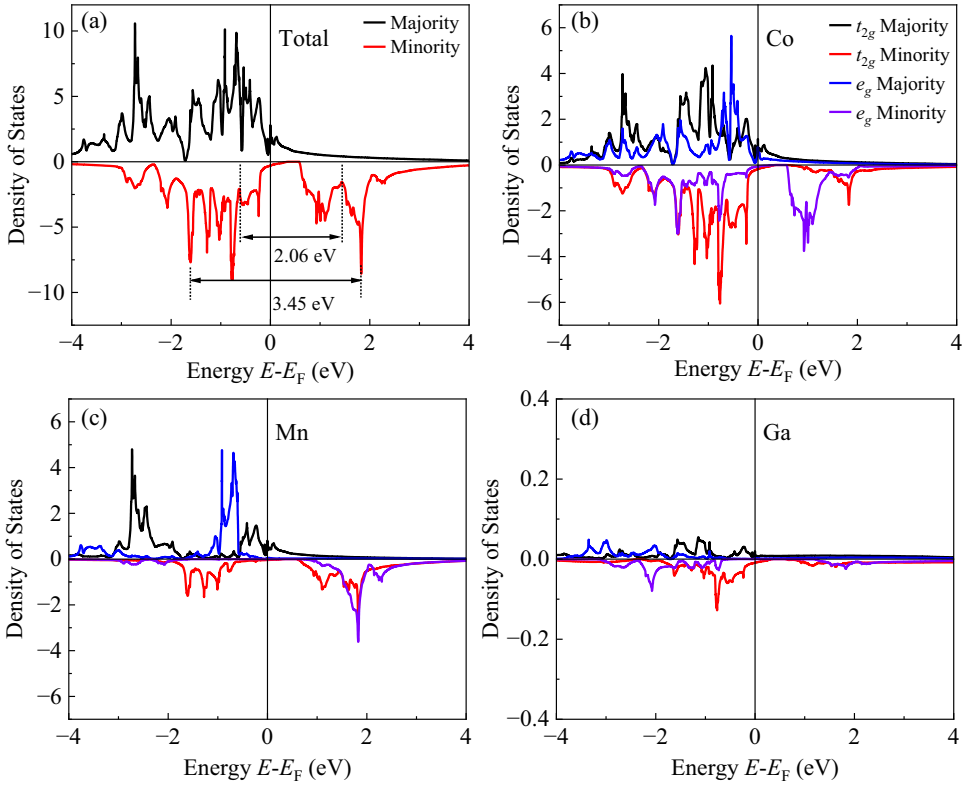

FIG. 3. Spin-dependent total (a) and element-resolved (b)–(d) densities of states for Co_2MnGa.

MCD(minority) − MCD(majority), the dominant minority spin contribution results in the giant MCD signal we observe.

The optical energy-excitation gap between the highest DOS regions ranges from 2.06 to 3.45 eV, which nicely matches our experimental results as shown in Fig. 1(b), where the lowest MCD signal is at 2.24 eV and the highest value at 3.50 eV. Thus our results suggest that the large UV MCD signal in Co_2MnGa thin films is due to transitions between these regions of the DOS. The element-resolved DOS [see Figs. 3(b)–3(d)] shows that Co and Mn atoms are the major contributors to the states involved.

D. Discussion

By comparing to previously reported MCD results of magnetic thin films in the UV region, including classic ferromagnetic transition metals and alloys, garnets, rare earths and oxides, the thickness normalized MCD in Co_2MnGa has a giant value, 36.2 mdeg/nm, as shown in Fig. 4(a). Though CoTb exhibits a large MCD as well, rare earth compositions such as this exhibit poor thermal stability [50]. Above 400 K, they can be crystallized and lose the amorphous structure, which ruins the magnetization and MCD effect, and thus limits their range of useable temperatures. Co_2MnGa, by contrast, has a higher Curie temperature $T_c \approx 700$ K [28], and combined with the temperature independence of its MCD signal it is an easy choice for practical applications at a wide range of temperatures.

The absorbance is a parameter showing how much light the sample absorbs, which is key for optospintronic applications. It is defined as $-\log T$, where T is the light-transmission ratio. We have characterized this information for Co_2MnGa with different thicknesses, as shown in Fig. 4(b). The absorbance increases with thickness, which is a typical behavior of metallic materials. Though the absorbance of 60.9-nm Co_2MnGa with giant MCD is more than 2.24 (0.57% light transmission) in the UV region, a commercial photodetector for CD spectroscopy is sensitive enough to detect the difference of the RCP and LCP absorption, even in this thick sample. On the other hand, the 7.6-nm Co_2MnGa thin film shows a relatively low absorbance of 0.54 (28.6% transmission) and still has a large MCD of almost 300 mdeg. Thus, in applications where the intensity of the transmitted light is key, thinner Co_2MnGa films can be integrated with other optoelectronic

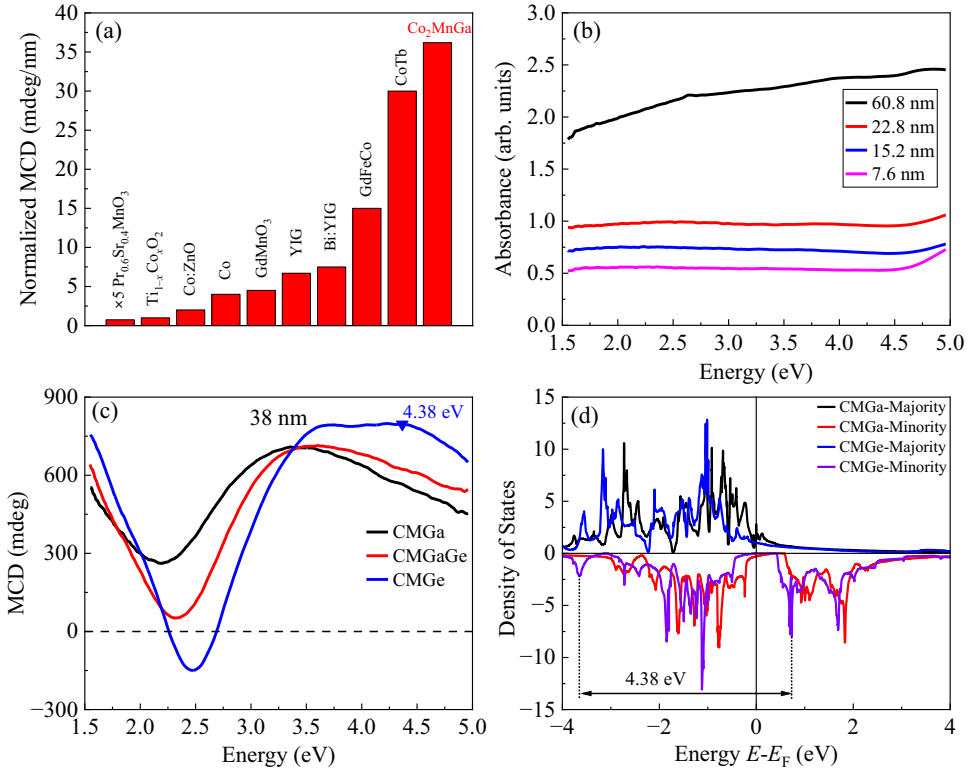

FIG. 4. (a) Comparison of thickness normalized MCD values for different materials $Pr_{0.6}Sr_{0.4}MnO_3$ [45], $Ti_{(1-x)}Co_xO_2$ [46], Co:ZnO [21], Co [22], $GdMnO_3$ [47], YIG [23], Bi:YIG [48], GdFeCo [49], and CoTb [49]. (b) Absorbance as a function of excitation energy for Co_2MnGa thin films. (c) MCD at 300 K as a function of excitation energy for 38 nm Co_2MnGa, $Co_2Mn(Ga, Ge)$, and Co_2MnGe. (d) Spin-dependent total densities of states for Co_2MnGa and Co_2MnGe.

devices, such as light-emitting diodes (LEDs), to control the helicity of emitted light [51].

Based on our results, we propose two rules to obtain large UV MCD using materials that are ferromagnetic or otherwise have spin-polarized band structures: (1) the difference in optical excitations between minority spin states and majority spin states should be very large to ensure a large MCD; (2) the regions in the DOS involved in these excitations should be separated by energies in the UV. To show evidence for these two rules, we characterized the MCD at 300 K in an alloy of $Co_2Mn(Ga, Ge)$, shown with the MCD for Co_2MnGa, $Co_2MnGa_{0.5}Ge_{0.5}$, and Co_2MnGe in Fig. 4(c). Co_2MnGe is a ferromagnetic Heusler alloy with the same crystal structure as Co_2MnGa. Both materials show very similar band structures, although the Fermi level in Co_2MnGe is slightly lower due to the presence of one additional electron per unit cell compared to Co_2MnGa [52]. One can see that replacing Ga with Ge to create the alloy results in a MCD signal that is higher in the UV region. More interestingly, Co_2MnGe shows a flat MCD from approximately 3.5 eV up to 4.38 eV. At the same time, adding Ge raises the valley of MCD from 2.20 to 2.48 eV. In addition, the polarization of MCD in the valley changes to the opposite direction for Co_2MnGe. These differences can be explained by the DOS differences in Fig. 4(d). Generally, the DOS of Co_2MnGe is very similar to that of Co_2MnGa but slightly shifted to lower energies, as Ge has one additional electron than Ga. However, in the Co_2MnGe DOS there is an extra peak located at -3.65 eV. These states are exactly 4.38 eV below the peak of unoccupied 3*d* states at $+0.73$ eV. This makes the energy excitation gap perfectly in line with the experimental results for the Co_2MnGe film where the MCD value is high right up to 4.38 eV.

It is worth mentioning that the dipole matrix elements are decisive for the probability of optical transitions [53]. This effect needs to be considered if there is a very high density of occupied states. For instance, though the unoccupied majority spin DOS is low in Co_2MnGe, the high occupied majority spin DOS at -1.01 eV below the Fermi level can significantly increase the probability of excitation, so that the CD originating from excitations between majority spin states may be higher than that from excitations between minority spin states, inducing the change of polarization for Co_2MnGe.

Based on the two rules, one can search for magnetic materials with specific band-structure features for achieving large MCD values at different energy-excitation regimes [54,55]. For instance, we expect other Co_2-based Heusler alloys, such as Co_2MnAl [56] and Co_2MnSi [57], to exhibit large MCD also based on their similar calculated band structures to those of Co_2MnGa and Co_2MnGe. Finally, it is also worth noting that the MCD signal in these Co_2-based Heusler alloys should also be nearly temperature independent due to their high Curie temperatures.

IV. CONCLUSION

We observed a giant temperature-independent MCD, 1450 mdeg, in the UV regime. The magnitude of MCD can be continuously changed to negative 1450 mdeg by sweeping the magnetic field. By calculating the spin-polarized DOS, we found that the MCD signal originates from the hybridization of Co and Mn 3*d* states. Based on our findings, we propose two rules for identifying magnetic materials with large UV-MCD: (1) the difference of minority and majority spin DOS should be very large; (2) the optical energy-excitation gap should be located in the UV region. We tested and confirmed these two rules in Co_2MnGe, which has a larger UV-MCD than Co_2MnGa, that we can clearly link to differences in the band structure. Beyond reporting a giant UV-CD response in a rare-earth-free ferromagnet, our study provides practical guidelines to discover and design thermally stable magnetic materials with large CD responses over various excitation energies.

ACKNOWLEDGMENTS

The MacDiarmid Institute is supported under the New Zealand Centres of Research Excellence Programme. This work is supported by the National Science and Technology Council, Taiwan, for financially supporting this research under Contract No. MOST 111-2112-M-153-002-MY3 21 and 112-2918-I-153-001. Y.Y. and N.M. gratefully acknowledge computational support from the NCI National facility at the Australian National University and Pawsey Supercomputing facility. Y.Y. and N.M. acknowledge the support from the ARC Centre of Excellence in Future Low-Energy Electronics Technologies (CE170100039).

DATA AVAILABILITY

The data are not publicly available. The data are available from the authors upon reasonable request.

[1] Y. Wang, J. Xu, Y. Wang, and H. Chen, Emerging chirality in nanoscience, Chem. Soc. Rev. **42**, 2930 (2013).
[2] B. P. Bloom, Y. Paltiel, R. Naaman, and D. H. Waldeck, Chiral induced spin selectivity, Chem. Rev. **124**, 1950 (2024).
[3] Y.-H. Kim, Y. Zhai, H. Lu, X. Pan, C. Xiao, E. A. Gaulding, S. P. Harvey, J. J. Berry, Z. V. Vardeny, J. M. Luther *et al.*, Chiral-induced spin selectivity enables a room-temperature spin light-emitting diode, Science **371**, 1129 (2021).
[4] L. Xu, X. Wang, W. Wang, M. Sun, W. J. Choi, J.-Y. Kim, C. Hao, S. Li, A. Qu, M. Lu *et al.*, Enantiomer-dependent immunological response to chiral nanoparticles, Nature **601**, 366 (2022).
[5] P. Lodahl, S. Mahmoodian, S. Stobbe, A. Rauschenbeutel, P. Schneeweiss, J. Volz, H. Pichler, and P. Zoller, Chiral quantum optics, Nature **541**, 473 (2017).

[6] K. M. McPeak, C. D. van Engers, S. Bianchi, A. Rossinelli, L. V. Poulikakos, L. Bernard, S. Herrmann, D. K. Kim, S. Burger, M. Blome *et al.*, Ultraviolet plasmonic chirality from colloidal aluminum nanoparticles exhibiting charge-selective protein detection, Adv. Mater. **27**, 6244 (2015).

[7] S. Beaulieu, A. Comby, D. Descamps, B. Fabre, G. Garcia, R. Géneaux, A. Harvey, F. Légaré, Z. Mašín, L. Nahon *et al.*, Photoexcitation circular dichroism in chiral molecules, Nat. Phys. **14**, 484 (2018).

[8] D. Ayuso, O. Neufeld, A. F. Ordonez, P. Decleva, G. Lerner, O. Cohen, M. Ivanov, and O. Smirnova, Synthetic chiral light for efficient control of chiral light–matter interaction, Nat. Photonics **13**, 866 (2019).

[9] J. Hu, M. Lawrence, and J. A. Dionne, High quality factor dielectric metasurfaces for ultraviolet circular dichroism spectroscopy, ACS Photonics **7**, 36 (2019).

[10] Y. Liu, Z. Wu, D. W. Armstrong, H. Wolosker, and Y. Zheng, Detection and analysis of chiral molecules as disease biomarkers, Nat. Rev. Chem. **7**, 355 (2023).

[11] Y. Tang and A. E. Cohen, Enhanced enantioselectivity in excitation of chiral molecules by superchiral light, Science **332**, 333 (2011).

[12] E. Hendry, T. Carpy, J. Johnston, M. Popland, R. Mikhaylovskiy, A. Lapthorn, S. Kelly, L. Barron, N. Gadegaard, and M. Kadodwala, Ultrasensitive detection and characterization of biomolecules using superchiral fields, Nat. Nanotechnol. **5**, 783 (2010).

[13] J. B. Khurgin, How to deal with the loss in plasmonics and metamaterials, Nat. Nanotechnol. **10**, 2 (2015).

[14] V. K. Valev, J. J. Baumberg, C. Sibilia, and T. Verbiest, Chirality and chiroptical effects in plasmonic nanostructures: Fundamentals, recent progress, and outlook, Adv. Mater. **25**, 2517 (2013).

[15] Z. Han, F. Wang, J. Sun, X. Wang, and Z. Tang, Recent advances in ultrathin chiral metasurfaces by twisted stacking, Adv. Mater. **35**, 2206141 (2023).

[16] Y. Chen, X. Li, L. Jiang, Y. Wang, and J. Li, Nanokirigami/origami fabrications and optical applications, Appl. Phys. Lett. **124**, 160501 (2024).

[17] O. Kovalenko, M. Vomir, B. Donnio, J.-L. Gallani, and M. V. Rastei, Chiromagnetoptics of Au and Ag nanoparticulate systems, J. Phys. Chem. C **124**, 21722 (2020).

[18] F. Pineider, G. Campo, V. Bonanni, C. de Julián Fernández, G. Mattei, A. Caneschi, D. Gatteschi, and C. Sangregorio, Circular magnetoplasmonic modes in gold nanoparticles, Nano Lett. **13**, 4785 (2013).

[19] D. Caldwell, J. M. Thorne, and H. Eyring, Magnetic circular dichroism, Annu. Rev. Phys. Chem. **22**, 259 (1971).

[20] J.-X. Lin, Y.-R. Chen, S.-J. Sun, C.-K. Hu, B.-J. Chen, and H.-S. Hsu, Field-free magnetoplasmon-induced ultraviolet circular dichroism switching in premagnetized magnetic nanowires, ACS Appl. Mater. Interfaces **14**, 11895 (2022).

[21] J. Neal, A. Behan, R. M. Ibrahim, H. Blythe, M. Ziese, A. Fox, and G. Gehring, Room-temperature magneto-optics of ferromagnetic transition-metal-doped ZnO thin films, Phys. Rev. Lett. **96**, 197208 (2006).

[22] C.-H. Huang, H.-S. Hsu, S.-J. Sun, Y.-Y. Chang, P. Misiuna, and L. T. Baczewski, Extraction of magnetic circular dichroism effects from blended mixture of magnetic linear dichroism signals in the cobalt/scotch tape system, Sci. Rep. **9**, 17192 (2019).

[23] W.-H. C. Chien, J.-Y. Huang, J.-X. Lin, Y.-F. Liao, H.-W. Su, H.-L. Liang, S.-Y. Huang, Y.-D. Yao, and H.-S. Hsu, Low current densities toggle optical polarization switching in Pt/yttrium iron garnet magnetic heterostructures using energy resolution, Physica Status Solidi (RRL)–Rapid Research Letters **14**, 2000223 (2020).

[24] J. Qin, L. Deng, T. Kang, L. Nie, H. Feng, H. Wang, R. Yang, X. Liang, T. Tang, J. Shen *et al.*, Switching the optical chirality in magnetoplasmonic metasurfaces using applied magnetic fields, ACS Nano **14**, 2808 (2020).

[25] K.-J. Jeong, D. K. Lee, V. T. Tran, C. Wang, J. Lv, J. Park, Z. Tang, and J. Lee, Helical magnetic field-induced real-time plasmonic chirality modulation, ACS Nano **14**, 7152 (2020).

[26] J. W. Kim, N. H. Cho, R. M. Kim, J. H. Han, S. Choi, S. D. Namgung, H. Kim, and K. T. Nam, Magnetic control of the plasmonic chirality in gold helicoids, Nano Lett. **22**, 8181 (2022).

[27] F. Qi, L. Li, Z. Li, L. Qiu, Z. Meng, and Y. Yin, Magnetic/plasmonic hybrid nanodisks with dynamically tunable mechano-chiroptical responses, ACS Nano **17**, 1427 (2023).

[28] Y. Zhang, Y. Yin, G. Dubuis, T. Butler, N. V. Medhekar, and S. Granville, Berry curvature origin of the thickness-dependent anomalous Hall effect in a ferromagnetic Weyl semimetal, Npj Quantum Mater. **6**, 17 (2021).

[29] L. Leiva, S. Granville, Y. Zhang, S. Dushenko, E. Shigematsu, T. Shinjo, R. Ohshima, Y. Ando, and M. Shiraishi, Giant spin Hall angle in the Heusler alloy Weyl ferromagnet Co_2MnGa, Phys. Rev. B **103**, L041114 (2021).

[30] L. Leiva, S. Granville, Y. Zhang, S. Dushenko, E. Shigematsu, R. Ohshima, Y. Ando, and M. Shiraishi, Efficient room-temperature magnetization direction detection by means of the enhanced anomalous Nernst effect in a Weyl ferromagnet, Phys. Rev. Mater. **6**, 064201 (2022).

[31] M. Aoki, Y. Yin, S. Granville, Y. Zhang, N. V. Medhekar, L. Leiva, R. Ohshima, Y. Ando, and M. Shiraishi, Gigantic anisotropy of self-induced spin-orbit torque in Weyl ferromagnet Co_2MnGa, Nano Lett. **23**, 6951 (2023).

[32] B. Mallett, Y. Zhang, C. Pot, K. Van Koughnet, B. Stanley, R. G. Buckley, A. Koo, Y. Yin, N. V. Medhekar, and S. Granville, Using optical spectroscopy to probe the impact of atomic disorder on the Heusler alloy Co_2MnGa, Phys. Rev. Mater. **7**, 094203 (2023).

[33] L. Sheng, Y. Zhang, J. Wang, P. Chen, J. Hu, J. Xia, G. Lan, J. Chen, K. Yu, Y. Zhang *et al.*, Resonant anomalous Hall effect in a ferromagnetic Weyl semimetal, Appl. Phys. Rev. **11**, 011405 (2024).

[34] T.-P. Chen, J.-X. Lin, C.-C. Lin, C.-Y. Lin, W.-C. Ke, D.-Y. Wang, H.-S. Hsu, C.-C. Chen, and C.-W. Chen, Strong excitonic magneto-optic effects in two-dimensional organic–inorganic hybrid perovskites, ACS Appl. Mater. Interfaces **13**, 10279 (2021).

[35] See Supplemental Material at http://link.aps.org/supplemental/10.1103/h822-rw47 for MCD from MgO substrate.

[36] G. Kresse and J. Furthmüller, Efficiency of ab-initio total energy calculations for metals and semiconductors using a plane-wave basis set, Comput. Mater. Sci. **6**, 15 (1996).
[37] C. R. Cantor, P. R. Schimmel *et al.*, *Techniques for the Study of Biological Structure and Function* (WH Freeman San Francisco, New York, 1980).
[38] P. Webster, Magnetic and chemical order in Heusler alloys containing cobalt and manganese, J. Phys. Chem. Solids **32**, 1221 (1971).
[39] M. Berciu, R. Chakarvorty, Y. Zhou, M. Alam, K. Traudt, R. Jakiela, A. Barcz, T. Wojtowicz, X. Liu, J. Furdyna *et al.*, Origin of magnetic circular dichroism in GaMnAs: Giant Zeeman splitting versus spin dependent density of states, Phys. Rev. Lett. **102**, 247202 (2009).
[40] J. Hu, Y. Zhang, X. Huo, N. Li, S. Liu, D. Yu, J.-P. Ansermet, S. Granville, and H. Yu, Large anomalous nernst angle in Co_2MnGa thin film, IEEE Magn. Lett. **13**, 1 (2022).
[41] W. Zhao, Y. Zhang, Y. Yin, K. Xing, S. Zhou, A. Bake, G. Akhgar, D. Cortie, L. Chen, X. Wang *et al.*, Giant Berry curvature in amorphous ferromagnet Co_2MnGa, Matter **8**, 101988 (2025).
[42] Y. Zhang, G. Dubuis, E. Trewick, and S. Granville, Reversal behavior and stability of spin textures with different topologies in ultrathin films, Phys. Rev. B **110**, 224413 (2024).
[43] Y. Zhang and S. Granville, Two-channel anomalous Hall effect originating from the intermixing in Mn_2CoAl/Pd thin films, Phys. Rev. B **106**, 144414 (2022).
[44] G. Van der Laan and A. I. Figueroa, X-ray magnetic circular dichroism–a versatile tool to study magnetism, Coord. Chem. Rev. **277**, 95 (2014).
[45] I. Edelman, Y. Greben'kova, A. Sokolov, M. Molokeev, A. Aleksandrovskiy, V. Chichkov, N. Andreev, and Y. Mukovskii, Visible magnetic circular dichroism spectroscopy of the $Pr_{0.8}Sr_{0.2}MnO_3$ and $Pr_{0.6}Sr_{0.4}MnO_3$ thin films, AIP Adv. **4**, 057125 (2014).
[46] T. Fukumura, Y. Yamada, K. Tamura, K. Nakajima, T. Aoyama, A. Tsukazaki, M. Sumiya, S. Fuke, Y. Segawa, T. Chikyow *et al.*, Magneto-optical spectroscopy of anatase Tio_2 doped with Co, Jpn. J. Appl. Phys. **42**, L105 (2003).
[47] G. A. Gehring, M. S. Alshammari, D. S. Score, J. R. Neal, A. Mokhtari, and A. M. Fox, Magneto-optic studies of magnetic oxides, J. Magn. Magn. Mater. **324**, 3422 (2012).
[48] S. Mito, S. Kikuchi, Y. Ito, N. Ota, and M. Inoue, Influence of sputtered ZnO and Al: ZnO top layers on magneto-optic responses of yttrium iron garnet films, Crystals **8**, 396 (2018).
[49] J.-X. Lin, B.-J. Chen, S.-M. Hung, W.-H. Liao, M. Hehn, S.-J. Sun, Y.-Y. Chang, T. Hauet, J. Hohlfeld, S. Mangin, and H.-S. Hsu, Electrically modulated multilevel optical chirality in GdFeCo thin films, ACS Appl. Electron. Mater. **7**, 177 (2025).
[50] H. Bai, T. Xu, Y. Dong, H.-A. Zhou, and W. Jiang, Spin-torque switching in rare-earth-free compensated ferrimagnet Mn_4N films, Adv. Electron. Mater. **8**, 2100772 (2022).
[51] P. A. Dainone, N. F. Prestes, P. Renucci, A. Bouché, M. Morassi, X. Devaux, M. Lindemann, J.-M. George, H. Jaffrès, A. Lemaitre *et al.*, Controlling the helicity of light by electrical magnetization switching, Nature **627**, 783 (2024).
[52] A. Candan, G. Uğur, Z. Charifi, H. Baaziz, and M. Ellialtıoğlu, Electronic structure and vibrational properties in cobalt-based full-Heusler compounds: A first principle study of Co_2MnX (X= Si, Ge, Al, Ga), J. Alloys. Compd. **560**, 215 (2013).
[53] J. Mack, M. J. Stillman, and N. Kobayashi, Application of MCD spectroscopy to porphyrinoids, Coord. Chem. Rev. **251**, 429 (2007).
[54] M. Kolbe, S. Chadov, E. A. Jorge, G. Schönhense, C. Felser, H.-J. Elmers, M. Kläui, and M. Jourdan, Test of band structure calculations for heusler compounds by spin-resolved photoemission spectroscopy, Phys. Rev. B **86**, 024422 (2012).
[55] S. Dutta, S. N. Panda, A. Markou, C. Felser, E. Lesne, and A. Barman, Role of spin transport on ultrafast spin dynamics in magnetic Weyl semimetal (Co_2MnGa)/Pt heterostructures with high spin-mixing conductance, Adv. Funct. Mater. **35**, 2413194 (2025).
[56] I. Di Marco, A. Held, S. Keshavarz, Y. O. Kvashnin, and L. Chioncel, Half-metallicity and magnetism in the Co_2MnAl/CoMnVAl heterostructure, Phys. Rev. B **97**, 035105 (2018).
[57] H. C. Kandpal, G. H. Fecher, C. Felser, and G. Schönhense, Correlation in the transition-metal-based Heusler compounds Co_2MnSi and Co_2FeSi, Phys. Rev. B **73**, 094422 (2006).